IEEE Access
Multidisciplinary ⋮ Rapid Review ⋮ Open Access Journal

Received January 15, 2021, accepted January 28, 2021, date of publication March 9, 2021, date of current version March 16, 2021.

Digital Object Identifier 10.1109/ACCESS.2021.3064753

Deep Learning-Based Approach for Detecting Trajectory Modifications of Cassini-Huygens Spacecraft

ASHRAF ALDABBAS[1], ZOLTAN GAL[1], (Member, IEEE), KHAWAJA MOYEEZULLAH GHORI[2], MUHAMMAD IMRAN[3], (Member, IEEE), AND MUHAMMAD SHOAIB[3]

[1]Department of Information Technology Systems and Networks, University of Debrecen, 4028 Debrecen, Hungary
[2]Department of Computer Science, National University of Modern Languages (NUML), Islamabad 44000, Pakistan
[3]College of Computer and Information Sciences, King Saud University, Riyadh 11451, Saudi Arabia

Corresponding author: Ashraf Aldabbas (ashraf.dabbas@inf.unideb.hu)

This work was supported in part by the University of Debrecen, Hungary, under Project FIKP-20428-3/2018/FEKUTSTRAT, in part by the QoS-HPC-IoT Laboratory, and in part by the Deanship of Scientific Research at King Saud University under Project RG-1435-051.

ABSTRACT There were necessary trajectory modifications of Cassini spacecraft during its last 14 years movement cycle of the interplanetary research project. In the scale 1.3 hour of signal propagation time and 1.4-billion-kilometer size of Earth-Cassini channel, complex event detection in the orbit modifications requires special investigation and analysis of the collected big data. The technologies for space exploration warrant a high standard of nuanced and detailed research. The Cassini mission has accumulated quite huge volumes of science records. This generated a curiosity derives mainly from a need to use machine learning to analyze deep space missions. For energy saving considerations, the communication between the Earth and Cassini was executed in non-periodic mode. This paper provides a sophisticated in-depth learning approach for detecting Cassini spacecraft trajectory modifications in post-processing mode. The proposed model utilizes the ability of Long Short Term Memory (LSTM) neural networks for drawing out useful data and learning the time series inner data pattern, along with the forcefulness of LSTM layers for distinguishing dependencies among the long-short term. Our research study exploited the statistical rates, Matthews correlation coefficient, and F1 score to evaluate our models. We carried out multiple tests and evaluated the provided approach against several advanced models. The preparatory analysis showed that exploiting the LSTM layer provides a notable boost in rising the detection process performance. The proposed model achieved a number of 232 trajectory modification detections with 99.98% accuracy among the last 13.35 years of the Cassini spacecraft life.

INDEX TERMS Cassini-Huygens interplanetary project, complex event, sensory data, big data, neural network, pattern processing, knowledge representation.

I. INTRODUCTION

Cassini spacecraft launched in October 1997 from the Earth arrived at Saturn on the 1st of July 2004 [1]. This event is named Saturn Orbit Insertion (SOI) of the spacecraft Cassini-Huygens. It required the spacecraft 6.7 years from the Earth's launch to reach its orbit around Saturn starting with SOI. The flybys generated by the gravity-assistance of the various planets are intended to boost the spacecraft's velocity proportionally to the Sun. Cassini also derives benefit from Saturn's biggest moon's gravity Titan, to be as a pivot point in favor of its major trajectory modifications [2]. Cassini's prime engine was required to slow down or stop the spacecraft by using a brake and allow Cassini to be situated into Saturn orbit upon the approaching in middle of 2004. The flight path of the orbiter was disposed to move away from the Saturn rings plane. This variation concerning the viewing geometry drove many unprecedented findings of formerly invisible ring kinetics and their atmospheric events, especially that take place at poles of Saturn.

The connotation of a complex event is tied up with the matters of processing multiple events accompanied by paying

The associate editor coordinating the review of this manuscript and approving it for publication was Deyu Zhang.

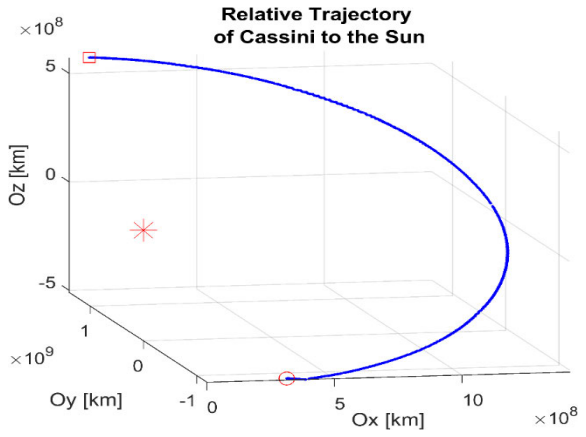

FIGURE 1. Cassini large-scale trajectory around the sun. The trajectory represented contains just the last 13.5 years, including the approaching phase, SOI event, and orbiting around the saturn of the cassini spacecraft. This interval is approximately half the period time of the saturn trajectory around the sun. starting point, ending point and sun are represented by circle, square and star markers, respectively.

attention to mark out distinct events within a timely tributary of events [3]. There are cases where the obtainable information to depict any process or system is just an inspection of the observations. For the scope of big data, there is a remarkable denomination of the issue, which is to recognize an extreme event [4]. Deep space discovery and interstellar flight, warrant a high degree of sophisticated analysis as it involves a high volume of events that need to be detected. Recent advancements in data collection volume from planetary space missions have facilitated new data science techniques. Cassini project obtained hundreds of gigabytes of scientific evidence which is extremely difficult to process through conventional means.

Machine Learning (ML) can help scientists operate on this larger-scale evidence. This curiosity derives mainly from a need to use ML to appreciate dynamic planetary structures better. However, spacecraft mission data are fundamentally difficult to integrate, for example, the unique Spatio-temporal existence of sampling into ML models. In order to establish a suitable mapping between incorporating the collected spacecraft data with ML approaches to reach an efficient ML algorithm, which iteratively learns from data, enables computers to detect hidden insights without being guided to search for them. We seek to detect offline events that are related to Cassini spacecraft trajectory modifications. This has motivated us, as there are complicated procedures needed for offline event detection techniques. This detection process is the most effective for the retrospective case.

The large-scale visualization in Fig. 1 represents the last 393,977 trajectory samples of the Cassini's flight path, which took place after the SOI event. This last 13.5 years of the trajectory, represented by approximately semi-ellipse in the large-scale representation, start with a circle shape in the bottom, while the square on the top symbolizes the end of the trajectory on the 14 of September 2017. On large-scale view, details of the Cassini orbit around Saturn are not visible and follow orbit of the Saturn around Sun. The Sun, the first sample, and the last sample are marked with a star, circle, and square characters, respectively. It should be mentioned that the trajectory of the Cassini after the SOI is a complex curve compound by an ellipse-based helicoid around the Saturn, which moves on the own ellipse curve around the Sun.

Fig. 2 shows Cassini trajectory for the last 4k samples, the starting point and ending point is represented with circle and square, respectively. Gaps of the plotted helicoid trajectory should be observed because of the non-periodic sampling process controlled by the Earth's project team. This makes it non-trivial to detect modifications of the trajectory. At the time Cassini moved comparatively approaching Titan, this moon gravitational impact snatched Cassini and swung it all over in an acute turn. If the spacecraft carried out a flyby with a higher altitude, then Titan's grip is baggy, and the Cassini trajectory is changed less.

If Cassini's moves by the southern hemisphere of Titan, then Cassini's path is on top of the rings of Saturn plane, which is toward the north comparative to Saturn's equator. If the spacecraft passed atop of Titan's north, then its path is sharply curved or having an angle southward, compared to Saturn.

Within this scope, Titan performed as a hub index for Cassini. Ordinarily, Cassini utilized propellant to create slight corrections that solicited it back in the direction of its purposed and optimal trajectory (known as ''reference trajectory'') regarding the subsequent Titan flyby. Also, every Titan flyby was destined to provide Cassini with the correct velocity and direction concerning its next Saturn orbit, enduring from one week to a few months, over which it could detect a specific rings or moons of Saturn. If the spacecraft is out of its course by to the extent of one kilometer, then Cassini should burn a small amount of propellant to put right the fault.

This paper examines the application of deep learning (DL) techniques to core big data analytics issues, motivating more focused analysis by specialists in these two fields. For this aim, we put forward our model that utilizes Long-Short Term Memory (LSTM) neural networks to elicit valuable data, learn the time series inner data pattern, and exploit the LSTM potential regarding memory dependencies. LSTM has been effectively used for trajectory prediction, but has never been employed by other research team for detecting spacecraft trajectory maneuvers modifications.

Among our contributions, we establish a suitable mapping between incorporating the collected spacecraft data with ML algorithm to detect automatically hidden insights without being guided to search for them. As far as we know, this research is the first one, which deals with detecting the events of spacecraft trajectory modifications. We concentrate our interest on detecting trajectory modifications of the orbiter Cassini. Should mention that time interval between SOI and end of Cassini project is 13.35 years, during we analyzed data to find trajectory modifications.

The rest of this paper is organized in the subsequent order: in the following section, we provide a brief

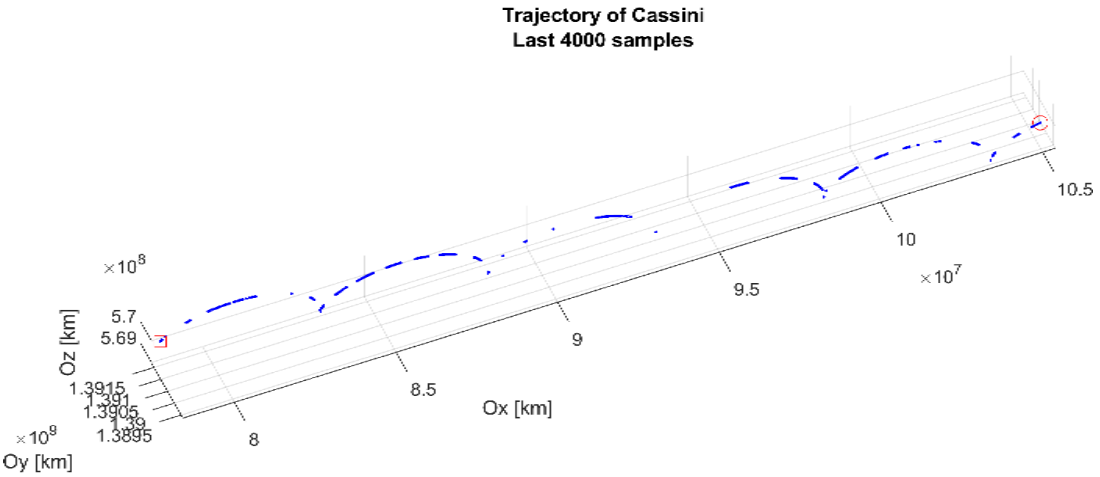

FIGURE 2. The last 4000 samples of cassini's small-scale trajectory. Sampling of the coordinates are not periodic, creating gaps on the sensed trajectory. First and last samples of this sampled sequence is represented by circle and square markers, respectively.

literature overview of several related studies within the field. Section III describes the extraction of sampling and trajectory characteristics of the NASA/Cassini database. Section IV discusses spacecraft trajectory modifications detection by LSTM-based algorithm along with the adopted method for the detection and results analysis. Section V contains the trajectory maneuvers detection's experimental results, and section VI summarizes our research conclusions.

II. RELATED WORK

ML is being widely utilized in energy and remote sensing applications. These applications include prejudice correction, robot controls, and more advanced evaluations. Algorithms and methods that will help machines to learn are used in ML. The key goal of ML is to extract knowledge by big data analytical methods efficiently. Trajectories taken by the Cassini mission can be split up into three groups of events occurring within phases: i) launch and convey to Saturn surrounding; ii) close in and arrive at Saturn orbit, and the iii) science phase. Launch and convey could utilize a tremendous amount of trajectory varieties with a span of various features like a specific phase duration, and velocity. Close-in and arrival phase would give the full particulars of the mission trajectory.

While in the science phase, the essential function of trajectory maps is to put the spacecraft on Saturn's particular place, which is meticulously designed and come up with suitable entry conditions connected with path angle and velocity. Essential attributes of the planet Saturn and Cassini's mission aims were integrated to provide an extent elasticity regarding selecting the science phase trajectory. The authors in [6] utilized an approach to specify the Rev-15 non-targeted Tethys flyby altitude, impelled via the navigational demands and operational restrictions, besides too many carried out trajectory modifications in order to minimize the gross Δv costs. The study in [7] presents the latest scientific highlights regarding the orbiter Cassini mission discoveries remodeling and principally modifying our understanding of this one of a kind planetary framework. In the last part of 2016, one of the Titan close flybys modified Cassini's trajectory forming a series of twenty rings forming remarkable orbits. These orbits comprise adjacent flybys of tiny moons.

Jason *et al.* [8] conducted an analysis of Cassini's trajectory comprising the 1st and the 2nd Titan encounters and portraying orbit determination through a dynamic approach and estimating the parameters related to the depiction of the final trajectory. The authors in [9] surveyed the trends of artificial intelligence (AI) in spacecraft control and guidance dynamics and concentrated on the evolutionary streamline and deep learning as it is the key for future systematic investigation in the space field. This is done by incorporating AI and automated reasoning to control the outer space mission trajectories navigation and remote sensing refinement. In paper [10], Support Vector Machine is utilized to identify trajectories accompanied by various movements among the distinctive trajectory modality, such as deviating events.

Up to recently, prior researches in aerospace that include massive data sets were imposed to utilize techniques that are less eligible for modeling impermanent or temporal data. LSTM is an artificial recurrent neural network (RNNs) that appoints a great hop toward aptly processing past events information and predicting the future. This type of neural network includes a weighted self-loop constrained with a circumstance that permits it to forget former information besides stockpiling it. The ingrained features of LSTM offer a typical candidate for extreme events detection, including any stream of data and time series. LSTMs are eligible to detect the interconnection among previous and current data, also appointing that connection in the mode of memorized or learned weights [11]. The trajectory prediction approach, termed as a grey dynamic filter, which merges dynamic measurement theory and the theory of grey system is suggested according to Qiyue *et al.* [12], an emulation of symmetric/asymmetric accelerated motion carried out.

One of the research papers introduces a trajectory prediction approach depending on the induced information assembling factor, intending to recognize the delicate spacecraft

TABLE 1. Tasks time stamps of main phases (UTC).

Task	Starting Date	Ending Date
C-H Project	15 October 1997	15 of September 2017
Analyzed DB	6 February 2004	15 of September 2017
Prime mission	1 July 2004	1 July 2008
Equinox mission	1 July 2008	11 October 2010
Solstice mission	11 October 2010	15 September 2017

TABLE 2. Number of saturn orbits and maneuvers.

Mission Name	Number of Orbits	Trajectory Maneuvers Planned	Trajectory Maneuvers Executed
Prime	75	161	112
Equinox	64	104	70
Solstice	155	206	141

trajectory prediction with interlocking arcs handed over by various equipment. It proposes the scope of induced harmonic median operator [13]. In [14], Gated Recurrent Unit (GRU) periodic neural network algorithm is provided for actual time trajectory prediction, where its parameters are acquired via batch processing as an initial phase, then the trained input for trajectory prediction. Silvestrini Stefano and Michele Lavagna [15], a model-based reinforcement learning is used to execute almost quintessential reconfiguration in establishing flying spacecraft. Along with two other algorithms, the LSTM layer network and inverse reinforcement learning are exploited to remodel and predict future trajectories in order to acquire collision-free maneuvers. These merits have inspired us to utilize the LSTM networks where the LSTM approach fits our research area.

III. EXTRACTING SAMPLING AND TRAJECTORY CHARACTERISTICS OF THE CASSINI-HUYGENS DATABASE

The spacecraft had two parts: Huygens probe and Cassini orbiter, Cassini-Huygens (C-H) arrive at orbit around Saturn in 2004, transmitting precious data back to the Earth. Huygens step inside Titan's atmosphere, the massive moon of Saturn, fall downward through a parachute to the furthest point so far, land on its surface, take samples, analyze them, and send the results to Cassini, forwarded them later to the Earth. Cassini instruments of remote sensing collected data remotely from enormous distances. The propagation time of the electric signal between the Earth and Cassini took around 80 minutes. After twenty years spent in outer space, the orbiter "Cassini" drained out of energy. Cassini was immersed into the atmosphere of Saturn on 15 of September 2017, and this is how the mission ended. The acquired images data was generated by the Imaging Science Subsystem (ISS) of The National Aeronautics and Space Administration (NASA). The ISS is composed of 2 detached cameras wide-angle camera and a narrow-angle camera. ISS image volumes dataset is composed of a huge number of images and their related labels, which hold the metadata of the images. The data set is publicly available at [5].

The 116 volumes of the data set analyzed by us were downloaded from the NASA source mentioned above. These 116 volumes contain last 13.5 years data sampled from Cassini. The altogether data set capacity is over 400 GB in compressed format and contains not only pictures but several other sensor values (e.g., temperature, position, velocity, angles, and identifiers). The staring sample has time stamp 02:07:06 on the 6th of February 2004, and the end stamp is at 19:59:03 on the 14th of September 2017, both explained in UTC (Coordinated Universal Time). The most important events of the project are summarized in Table 1.

During the five main objectives of the C-H project (i.e., research of Saturn, moon Titan, rings of Saturn, icy satellites, and magnetosphere measurements), there was necessary execution of trajectory maneuvers. The number of planned and executed modifications of the trajectory for each mission is provided in [16].

The ratio of the number of executed and planned trajectory maneuvers is 69.5% and 67.3% for the Prime and Equinox mission, respectively. Having no official information about the executed trajectory modifications in the Solstice mission, our prognosis is 68.4% (average of the previous two) of the planned maneuvers, giving a number of 141 trajectory modifications. Table 2 provides the number of Saturn orbits along with the planned and executed maneuvers.

The invariable reference system concerning the planetary framework is the plane crossing over its barycentre, known as the center of the mass. Relatively the most percentage of this effect is due to the mass of the biggest four gas planets: Uranus, Jupiter, Saturn, and Neptune. The Sun composes the counterpoise of all of our solar system planets. Therefore, it is close to the barycentre at the time that Jupiter is situated at one side while the other 3 (gas giants) are on the obverse side. The gross angular momentum could be realized via the invariable plane. The plane could be addressed as invariable (consistent) during the time that operational in Newtonian dynamics. Within our solar system, the angular momentum's overall vector is steady, corresponding to the spatial ordinate time.

Accordingly, the invariable plane [17] is described as the plane which is vertical to the overall angular vector of the quantity of motion of a moving body in the solar system, which moves over its barycentre. So, based on that being steady, it offers a perpetual instinctive reference plane, with the fact that the ecliptic partially shifts with time. As the possess orbital parameters of the Earth, and immanent motions are quite recognized, measurements of outer space orbiter motion, which is discerned visually from Earth, could be transformed into a Sun-centered parameterized path, which is required to characterize the trajectory of the spacecraft. The characteristics of the time difference Δt between consecutive samplings executed by Cassini can be seen in Fig. 3. The mean and standard deviation of the Δt is 1,053 seconds and 12,282 seconds, respectively.

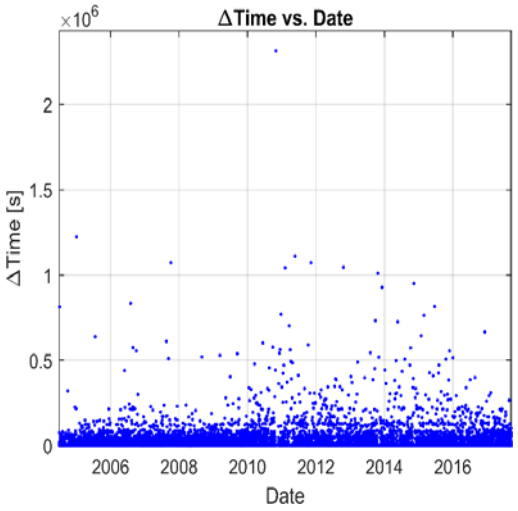

FIGURE 3. Characteristics of the consecutive sampling intervals at the cassini. Non-periodicity of sampling moments is based on the decision of management staff at the earth.

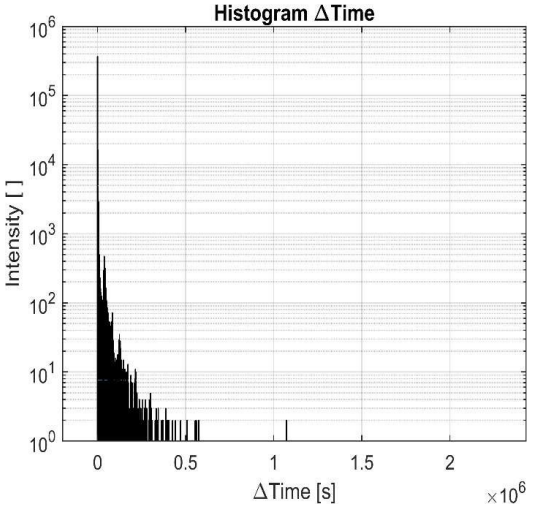

FIGURE 4. Histogram of the inter-sampling time intervals. majority of the intervals are shorter than 200,000 sec but there were few intervals in the scale of four days, as well.

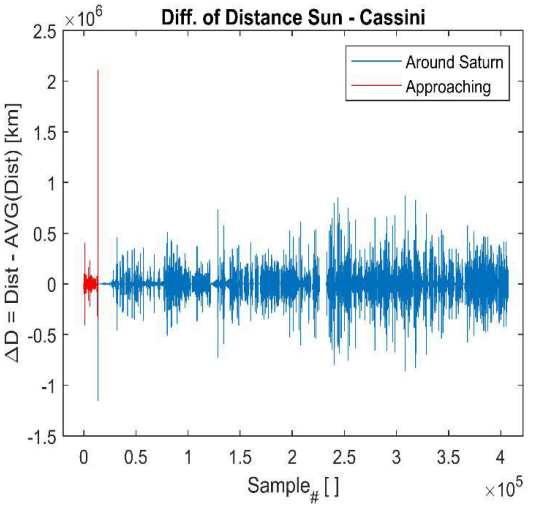

FIGURE 5. Difference of cassini-sun sampled distance and moving average distance, ΔD during the NASA whole database samples (13.5 years). The bubbled initial part represents the approaching phase, and the blue part shows the orbiting phase around saturn of the cassini.

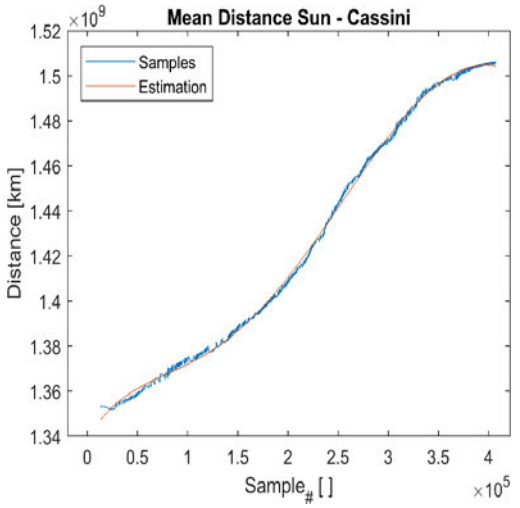

FIGURE 6. Mean distance sun-cassini in large scale during the NASA database (approx. half orbit time of saturn around Sun). Because of ellipse trajectory of saturn around Sun the moving average distance of sun-cassini is a distorted sinus function in interval scale $(-\pi/2, \pi/2)$ which can be approximated by a polynome.

Fig. 4 represents the distribution of the sampling intervals at the Cassini. To have a frequency distribution of an occurrence within a relevant interval of consecutive sampling. The relative frequency is proportional to the observed frequency of a data value divided by the sample size. C-H data set downloaded from the NASA web site contains N = 407, 303 samples. These samples refer to the last 13.5 years of the interplanetary mission in the time interval [16-Feb-2004, 15-Sep-2017]. Data capturing were executed in different phases and sub-phases of the project.

Each sub-phase has several sequences where each sequence has a number of observations depending on the decision of project leaders. An observation contains a set of samplings where the set size depends on the technological events of the spacecraft or astronomical events around Saturn. The number of sequences and number of observations in the analyzed time period by us was 2,355 and 10,851, 10,851 respectively. Detailed information showing the analyzed data can be found in Table 3.

The sampling moments of the sensor values by the orbiter Cassini were not periodic during the project duration. Fig. 5 signifies the period that took place before the insertion and appears in bubbled, while the blue color represents the period after the insertion to Saturn orbit. This figure expresses the difference of Sun-Cassini distance and the average distance to the Sun over the last 13.5 years of the mission. We have shown the crossed trajectory by the spacecraft journey versus the sample number by providing the sampled and estimated distance between Cassini and the Sun. The gap in distance values between samples 225,900 (24-Jun-2010) and 232,800 (30-Aug-2010) is caused by the long duration of the data

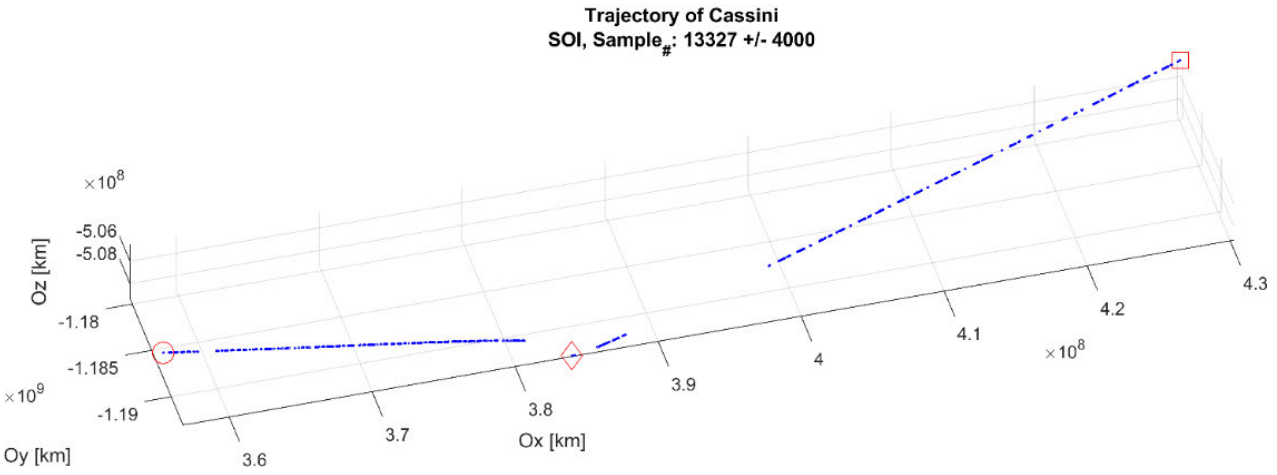

FIGURE 7. The medium-scale trajectory of cassini around the SOI process. The circle is the starting moment of the plotted interval (samples $13,327 - / + 4,000$). The diamond mark represents the insertion point (SOI: sample 13,327) of the cassini on orbit around saturn. Because of significant trajectory modification before SOI, the two parts of the plotted large-scale trajectory are evasive.

TABLE 3. Number of analyzed phases, sub-phases, sequences and observations.

Mission Name	No. of Analyzed Phases	No. of Analyzed Sub-Phases	No. of Analyzed Sequences	No. of Analyzed Observations
Prime	2	3	921	3912
Equinox	3	8	215	1991
Solstice	6	3	1219	4948

reception missing. This event looks to be most critical situation of this NASA project because no connection existed between Earth and Cassini for that weeks. The modification of the Sun-Cassini distance can be observed by the small spikes with amplitude in scale of 0.1 to 0.8 million kilometer.

While the mean distance between the Sun and Cassini over samples is given in Fig. 6, we estimated the average (large-scale) value of the Sun-Cassini distance, D versus the sample IDs by polynomial curve fitting. The smallest degree of the fitting polynome having an excellent coefficient of determination $R^2 = 0.999$ we have found to be five.

$$D(s) = \sum_{i=0}^{5} a_i \cdot s^i \tag{1}$$

The coefficients of the distance fitting polynome, $D(s)$, are listed in Table 4. It is obvious that should be high differences in the order of magnitude of coefficients belonging to different powers of the sample index. We have relatively small modifications in the high powers and oscillation of position of Cassini around the Saturn (see Fig. 1 and Fig. 5. as large-scale trajectory and deviation from average, ΔD).

To illustrate the change that is happening within Cassini velocity, we represent Fig. 7 [18], which gives details of the SOI process. The trajectory in a medium distance scale is a helicoid with an ellipse in cross-section view to the Saturn orbit. At the same time, an engine firing was initiated to decrease Cassini velocity. The maneuver of SOI took roughly

TABLE 4. Coefficients of the LARGE-SCALE distance fitting polynome, $D(s)$.

Coefficient	Value
a_5	$7.33 \cdot 10^{-20}$
a_4	$-9.86 \cdot 10^{-14}$
a_3	$4.14 \cdot 10^{-8}$
a_2	$-5.86 \cdot 10^{-3}$
a_1	$5.42 \cdot 10^{2}$
a_0	$1.34 \cdot 10^{9}$

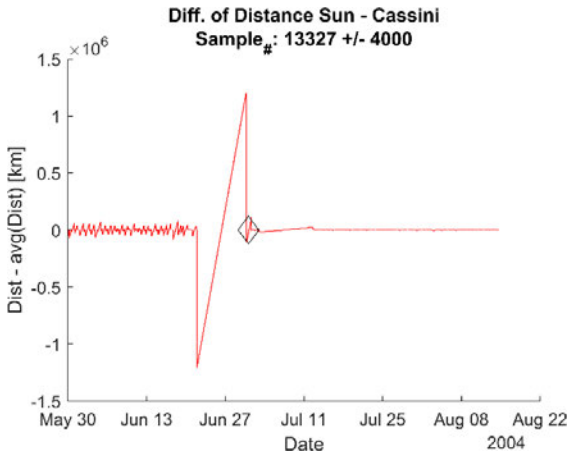

FIGURE 8. Difference of sun-cassini distance and moving average distance around the SOI process (samples $13,327 - /+ 4,000$) in function of time. The diamond mark represents the insertion point (SOI). Large spike before SOI represents data missing in the NASA public database. Small spikes in june 2004 are caused by possible inaccuracy of measurement.

ninety minutes, let the spacecraft be caught via Saturn's gravity and enter an orbit with five months period long. The red circle is the starting moment of the interval. The diamond mark represents the insertion point (SOI) of the Cassini around Saturn orbit.

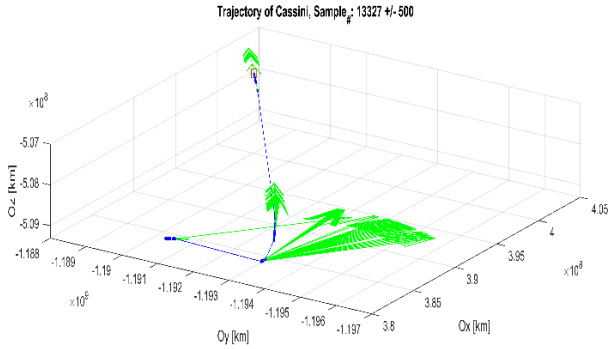

FIGURE 9. The small-scale trajectory samples of the cassini around the SOI (Sample# = 13,327). Segments between consecutive sampled positions help to track the movement of the orbiter and are not the real trajectory. Arrows represent direction of the instantaneous velocity.

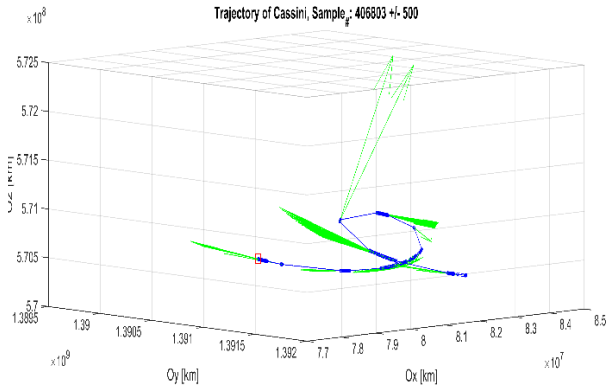

FIGURE 10. The small-scale trajectory of cassini in the last 1K sample. The square shows the last sample of the cassini. Green arrows show the direction and size of the instant velocity of the orbiter. Segments between consecutive sampled positions help to track the movement of the orbiter and are not the real trajectory.

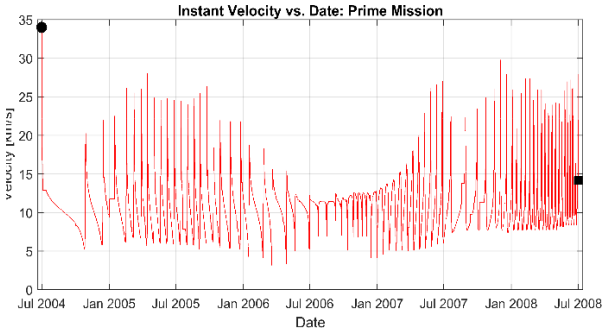

FIGURE 11. The magnitude of the instant velocity of the cassini to the solar system during the prime mission. The range of velocity component is between 4 and 35 km/s. Oscillation of the orbit is visible by the spikes.

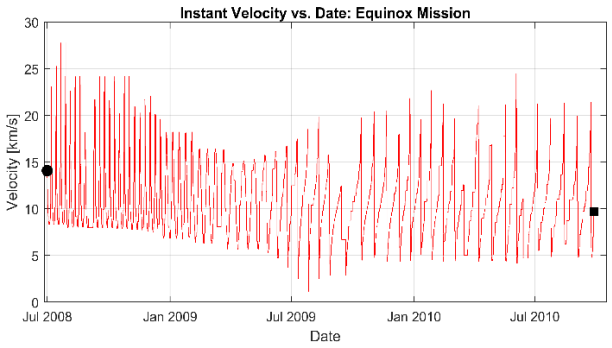

FIGURE 12. The magnitude of the instant velocity of the cassini to the solar system during the equinox mission. The range of velocity component is between 1.5 and 28 km/s.

As represented in Fig. 8, the Cassini spacecraft reduced its speed to get a successful insertion within the SOI maneuver. After the insertion, the spacecraft moved in a marginally elliptical orbit. Thus, the distance between the spacecraft and the Sun diverges. The consecutive discrepancy of the location values leaps really high in the satellite data records since only a few samples were deposited into the NASA database at this time.

A projection of Cassini's large-scale trajectory around the SOI and the last phase of the project in small-scale is given in Fig. 9 and 10, respectively. The square represents the last position in this interval. Green arrows show the direction and size of the instantaneous velocity. Dots are the sampled position of the spacecraft.

Small-scale fluctuations of the orbit can be observed, as well. The SOI maneuver started before the sample 13,328 of the NASA/Cassini database with 116 volumes. There were around 19 hours after the SOI without sampling. Fig. 10 depicts the position and velocity of Cassini to the Sun in the last 1000 samples of the project. Fig. 11-13 depict the velocity of Cassini to the Sun in the Prime, Equinox, and Solstice mission respectively. Velocity magnitude at the beginning and the end of each mission is represented with a black filled dot and square objects, respectively. The time interval between spikes of the curves represents the variable period of the helicoid orbiter around Saturn. The velocity of Cassini with respect to Saturn fluctuated from 12.5 km/s to 18.5 km/s conform to [19]. Our analysis is based on the NASA database resulted in velocity values to the solar system 3.18…29.75 km/s. Because the time period of Solstice mission was around seven years, the number of orbits around Saturn was higher (see Table 1.). The relatively small modifications of the velocity in the second half of 2013 are caused by the orbiter plan's specific relative position to the solar system.

IV. CONDITIONS OF THE COMPLEX EVENT DETECTION OF THE CASSINI TRAJECTORY

The trajectory is changed when the magnitude of the velocity vector v (v_x, v_y, v_z) is greater than a threshold Th_v for consecutive samples, or if the velocity angle changes between consecutive vectors. The main aim behind applying our classifier is to specify complex events from sensory generated data. For the purpose of detecting temporal semantics for complex event recognition, we prolonged the time index of the sensory data. Potential complex events of the data set are in the moment of change of observation sequences. We consider extreme modification of the trajectory when the Cassini orbiter velocity vector changes more than a threshold metric. Because the velocity is a measure vector, extreme events in the trajectory imply fulfilling any of the following two

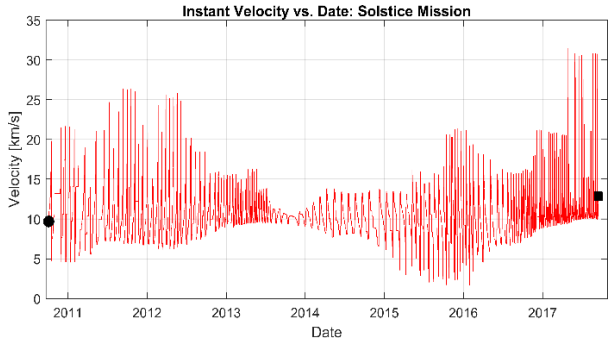

FIGURE 13. The magnitude of the instant velocity of the cassini to the solar system during the equinox mission.

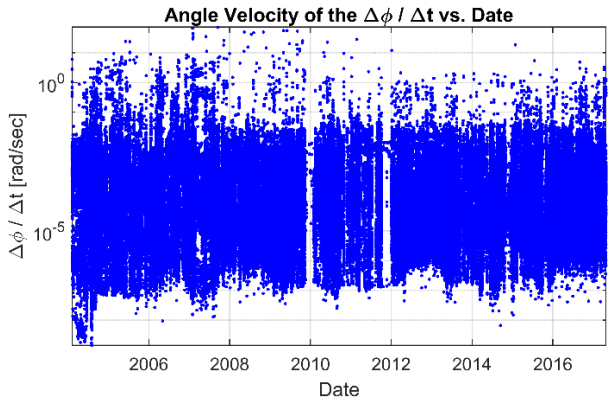

FIGURE 14. Angle modification per unit time of the consecutive velocity vectors of the cassini.

conditions: extreme modification of the velocity direction or the acceleration vector's magnitude. A fundamental purpose of implementing our classifier is to infer events from sensory evidence. Cardinality sets were used to give the number of extreme events considered trajectory modifications. Working points are represented with red bubble objects. Also, the Cassini positions during the trajectory modifications are provided.

A. MODIFICATION OF THE VELOCITY VECTOR DIRECTION

The velocity of the angle modification $\Delta\phi_i$ between consecutive velocity vectors v_i and v_{i+1} is given by the following formula:

$$\frac{\Delta\phi_i}{\Delta t_i} = \frac{acos\left(\frac{\overline{v_{i+1}}\cdot\overline{v_i}}{\|\overline{v_i}\|\cdot\|\overline{v_{i+1}}\|}\right)}{t_{i+1}-t_i}, \quad i = 1, 2, \ldots, N-1 \tag{2}$$

where $\overline{v_i}$ and $\overline{v_{i+1}}$ are two consecutive velocity vectors of the orbiter, $\|\overline{v_i}\|$ is the magnitude of the vector, Δt_i is the time interval between two consecutive samplings, and $i = 1, 2, \ldots, N-1$. The number of vectors is the total number of samples in the Prime, Equinox, and Solstice missions: $N = 407,303-13,326 = 393,977$. This number of samples analyzed by us belongs to the last 13.5 years of the C-H project. A value around 0 of the $\Delta\phi/\Delta t$ means a tiny modification of the direction per unit of time. Such cases were at the beginning of the project (see values before 2005 in Fig. 14). Starting with the SOI event, the angle of the consecutive

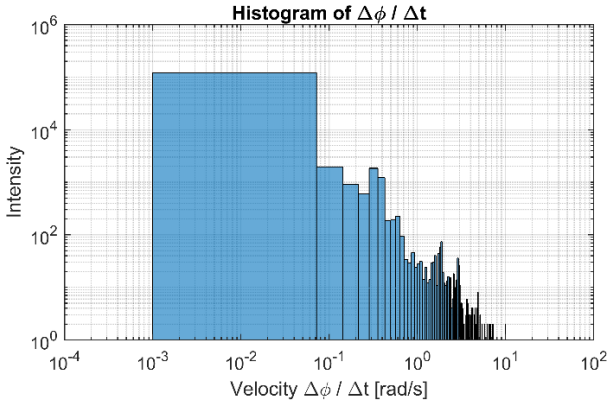

FIGURE 15. Histogram of the angle modification per unit time of the consecutive velocity vectors of the cassini.

samplings of the velocity direction modifies in a higher range per unit of time. The spacecraft trajectory was modified several times, but no detailed information is available publicly about these events. The accessible database of the NASA with 116 volumes contains samplings with high dispersion of the time.

Values of the $\Delta\phi/\Delta t$ in the scale of over 1 rad/sec were sampled in case of relatively short delay time between consecutive samplings. The distribution of the $\Delta\phi/\Delta t$ is exponential conform to the histogram of Fig. 15. The direction of the movement is changing just in a small range for most samplings, but there are cases when the direction changes more radically.

B. MODIFICATION OF THE ACCELERATION VECTOR MAGNITUDE

Modification of the trajectory is made when the magnitude of velocity vector v (v_x, v_y, v_z) modify by a greater value than the threshold Th_v during the consecutive samplings. Calculation of the modification magnitude per unit of time of the velocity vector between two consecutive samplings (being the acceleration) is based on the velocity components given on the NASA database conform to the following relations:

$$\overline{v} = \overline{v_x} + \overline{v_y} + \overline{v_z} \tag{3}$$

$$a_i = \frac{\|\overline{\Delta v_i}\|}{\Delta t_i} = \frac{\|\overline{v_{i+1}} - \overline{v_i}\|}{t_{i+1}-t_i}, \quad i = 1, 2, \ldots, N-1 \tag{4}$$

The magnitude of velocity modification can be derived using the following relation:

$$\|\overline{v_{i+1}} - \overline{v_i}\|^2 = (\Delta v_{x,i})^2 + (\Delta v_{y,i})^2 + (\Delta v_{z,i})^2 \tag{5}$$

where $\Delta v_{x,i}$, $\Delta v_{y,i}$, $\Delta v_{z,i}$ are the modification of the orthogonal velocity components in the sampling interval i, and $i+1$. The acceleration magnitude Cassini can be seen in Fig. 16.

Acceleration denotes a velocity change, either transmogrification within direction or speed or the two of them. At the time there is a change in the speed, then the force of inertial is orientated ahead (in case there is a decrease in speed) or rearward (in case there is an increase in speed). While during the time that there is a change in the direction, then with

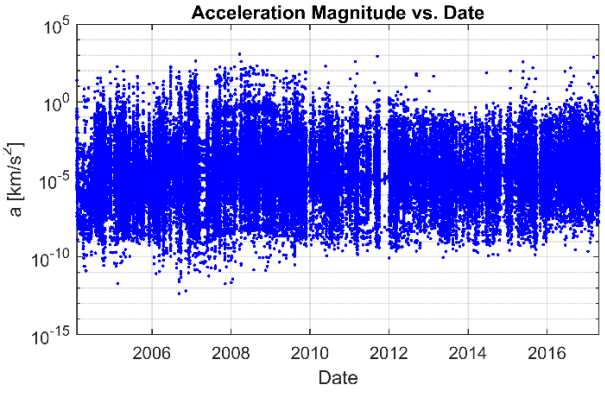

FIGURE 16. Acceleration magnitude of the cassini. The majority of the magnitudes of a are less than 1 km/s^2.

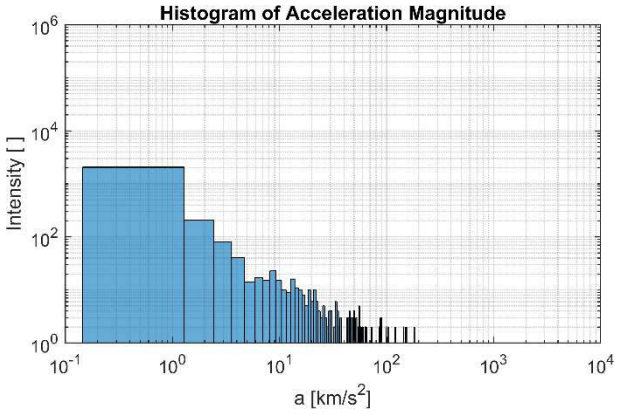

FIGURE 17. Histogram of acceleration magnitude of the cassini.

this case, the force of inertial is oriented in the direction to left (in the case of right rotation) or in the direction to right (in the case of left rotation). Distribution of the acceleration magnitude in Fig. 16 is the power function that conforms to the histogram of Fig. 17.

The histogram denotes a method in which the intensity of acceleration events gauged within a particular magnitude period is distributed throughout potential magnitude values. Every level within the generated histogram expresses the rate of acceleration counts taking place among the acceleration span. The log-log scale histogram can be approximated by a linear function, a resulting power function dependence of the histogram for acceleration.

C. COMPLEX EVENT DETECTION OF THE CASSINI ORBITER TRAJECTORY

An essential purpose of implementing our classifier is to infer events from sensory evidence. For the intent of complex event identification of the temporal semantics associated with complex event recognition, we extended the length of the sensory results. The occurrences that can be detected are the dynamic shifts from the set, as given by the moments of transition in observation sequences. Let have the indexes of trajectory modification where special events given by set I:

$$I_\phi = \left\{ 1 < i < N-1 \left| \frac{\Delta\phi_i}{\Delta t_i} \geq Th_\phi \right. \right\} \tag{6}$$

$$I_a = \{1 < i < N-1 | a_i \geq Th_a\} \tag{7}$$

$$I = I_\phi \cup I_a \tag{8}$$

$$J = I_\phi \cap I_a \tag{9}$$

where I_ϕ and I_a are sample indexes of the analyzed NASA database for which the velocity direction modifications or the acceleration magnitude are greater than the corresponding threshold values. Set J is used to sense the individual effect simultaneously of the two conditions mentioned in subsections IV.A and IV.B. If the cardinality of the set J is high, then these two conditions are not strongly dependent and help to detect complex events on the trajectory. The resulting set I contains all the sampling indexes detected by the proposed

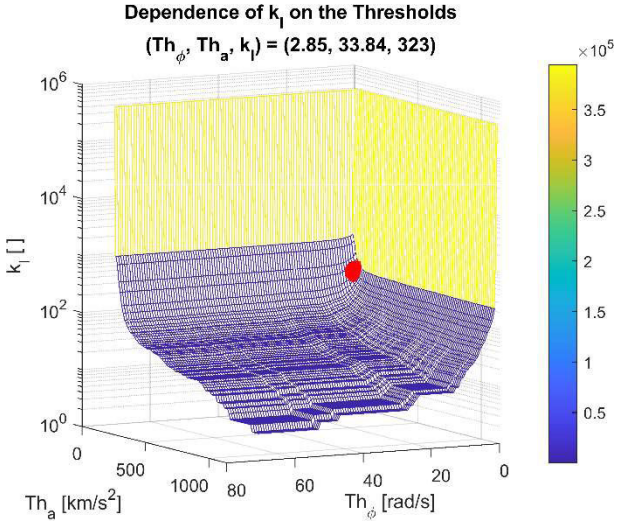

FIGURE 18. Dependence of the cardinality of sets I (a) and J (Φ).

complex event detector.

$$I = \{i_1, i_2, \ldots, i_k\} \tag{10}$$

After the process of SOI in 2004, the spacecraft was executing several modifications of the trajectory conform to the commands sent by the supervisor team from the Earth. By exploiting dependency of the number of extreme values on the threshold values Th_ϕ and Th_a within our model, we are able to determine the working point in three-dimensional space. Fig. 18 sets out this dependency as a surface plot. Cardinality k_I and k_J of the sets I and J, respectively, give the number of extreme events considered trajectory modifications of the Cassini based on the detection conditions (6) or (7) during the analyzed last 13.5 years of the project.

It is obvious that the trajectory modifications executed should be less than the number of observations mentioned in section 3, $M = 10,851$. Based on Table 1., the number of executed maneuvers was considered to be 323. The working point on both surfaces is placed on ordinates with extreme modification of the surfaces. To fulfill the total number of trajectory maneuvers, the values of the thresholds are $(Th_\phi, Th_a) = (2.85\ rad/s, 33.84\ km/s^2)$. For these threshold

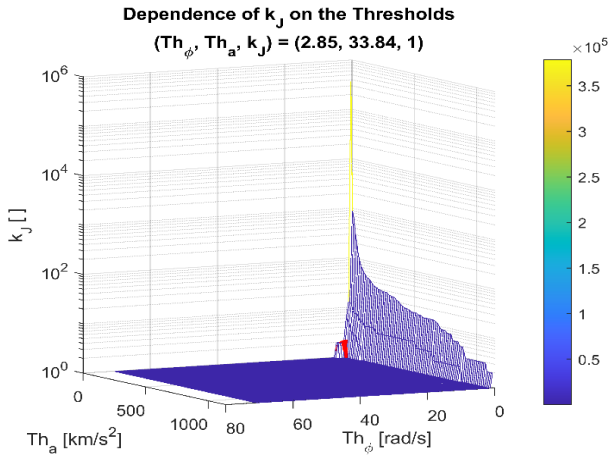

FIGURE 19. Dependence of the cardinality on Th_ϕ and Th_a.

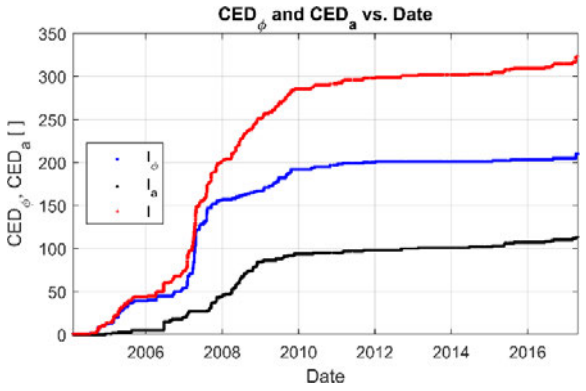

FIGURE 20. Complex events of the cassini trajectory vs. date. curves in increasing order of the height are I_a. I_ϕ, and I respectively.

values, the cardinality of the set I and J were found to be $(k_I, k_J) = (323, 1)$. Fig. 19 gives the dependence of the cardinality on the thresholds Th_ϕ and Th_a.

The representation of complex events detected in the set I_ϕ and I_a are given in Fig. 20. The total number of extreme events based on velocity vector modification and acceleration magnitude modification is 210 and 114.

The working points are represented with red bubble objects and are placed in the extreme modification points of the gradient of the surfaces. It can be assumed that approximately two times more extreme events appear in the set I_ϕ than in the set I_a. The majority of the trajectory maneuvers were executed in the Prime mission, and a relatively small number of modifications were done in the last, Solstice mission. The cardinality of sets I_ϕ and I_a in the function of time have a ratio of approximately 2/1.

These two sets are not disjunctive because, in several samples, both detection conditions (6) and (7) fulfill. The union of these two sets gives precisely the number of 323 extreme events of the trajectory modifications. In continuation, we show the method to detect these trajectory maneuvers with supervised recurrent neural networks.

The positions of the Cassini orbiter during the trajectory modifications are represented in Fig. 21. The physical

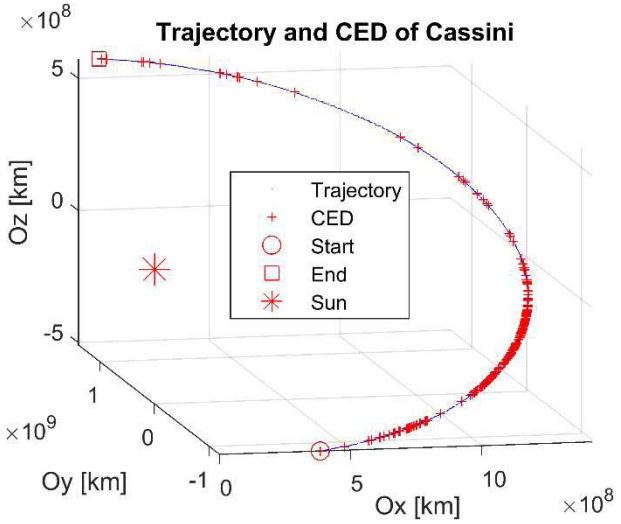

FIGURE 21. Cassini positions during the trajectory modifications.

position of Complex Event Detections (CEDs) in the solar system shows that majority of maneuvers were executed in the first mission (Prime). The Sun, the first sample, and the last sample are marked with a star, circle, and square characters, respectively.

V. DEEP LEARNING FOR DETECTION OF SPACECRAFT TRAJECTORY MODIFICATIONS

The aspect of acquirements with ML indicates the aptitude of an algorithm to notice and memorize patterns among data to ameliorate the results, i.e., to utilize the existing data so that we can foretell events and solve the ambiguity. AI already has an implementation in many fields such as aviation, speech recognition, and classification [20]. The technology is foreseeable to consolidate future outer space exploration since it could process big datasets volumes, detect patterns in image datasets, and specify spaceship status.

AI has become an effective method to find an answer to change detection or CED. DL has the ability to control spacecraft regarding handling geometric positions within a relatively low timeframe via the increasing ability to create neural networks capable of solving complex pattern recognition problems and learning curves on any form of geometric surface. Just as space missions are ever more frequent, intricate, and spacecraft to be sent away distance from Earth, there shall be an increasing request for rapid and automatic-adjusting machine learning established navigation potency. The scope may comprise orbit adjustment and self-directed navigation. We developed a recurrent neural network and trained it to find such events based on CED.

Embedding layers of the neural network are exploited to include vectors, which have a high point or dimensionality level. The LSTM layer passes the embedding layer as input and offers a greater abstraction scope for each data object. The memory gating method established in LSTM has turned the recurrent neural network into a robust mechanism to encode and seize long-term dependency. The stacked

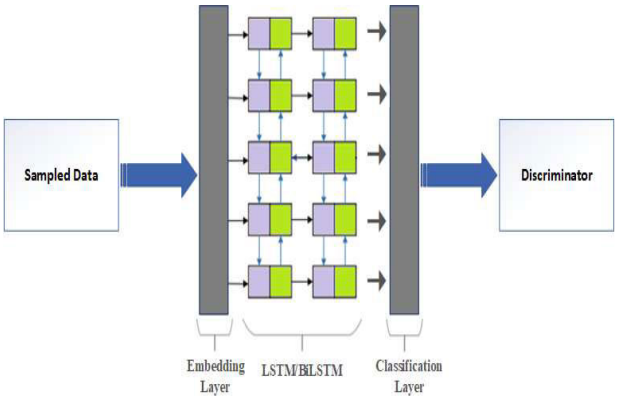

FIGURE 22. General architecture of the used LSTM networks.

approach of LSTM can be considered as an expansion of the LSTM model, having numerous hidden layers in which every recurrent layer includes several memory cells. The aim of utilizing multiple layers of LSTM is to impart more innovative data allocations.

We utilized one RNN layer approach in which the output of the preceding LSTM layer is forwarded as input for the following layer (see Fig. 22).

The classic characteristic of RNN architecture can be the periodic connection, and this qualifies the RNN to have the ability to update or refurbish the present state depending on the previous states besides the present input data [21].

A. DEEP LEARNING METHOD OF DETECTING TRAJECTORY MODIFICATIONS

Based on the work provided in [22], the way in which two or more concepts or objects are connected among the orbital elements would help to analyze the impact on spacecraft trajectory. The efficient analysis of any framework entails the empirical observations reference in the time domain. The proposed approach is an amalgamated framework, which can specify trajectory modifications among the mission of the C-H expedition. The analysis of trajectories gives the opportunity to acquire information, not just about the spacecraft motion, but allows gaining a better motion analysis based on ML.

The provided framework in this research paper captures the trajectories as inputs and analyses them temporally and spatially, depending on the sample number and timing of that samples beside the spacecraft velocity.

The input to the RNN system is a sequence of sample ID $i \in \{1, \ldots, N-1 = 393,976\}$, sampling intervals $\Delta t_i = t_{i+1} - t_i$, modification of the position coordinates $(\Delta x_i, \Delta y_i, \Delta z_i)$ and modification of the velocity components $(\Delta v_{x,i}, \Delta v_{y,i}, \Delta v_{z,i})$ among the last 13.5 years of the studied time interval. The input of the neural network is a $7\,x\,N$ matrix X conforms to the formula below:

$$X = [X_1, X_2, \ldots, X_{N-1}] \tag{11}$$

where the column vectors X_i have the following elements:

$$X_i = \left[\Delta t_i, \Delta x_i, \Delta y_i, \Delta z_i, \Delta v_{x,i}, \Delta v_{y,i}, \Delta v_{z,i}\right]^T \tag{12}$$

TABLE 5. Dimension features of the data subsets.

Data subset	Start index	End index	Matrix dimension
XTrain	1	$(N-1)/2$	$7\,x\,(N-1)/2$
YTrain	1	$(N-1)/2$	$7\,x\,(N-1)/2$
XValidate	$(N-1)/2+1$	$3\cdot(N-1)/4$	$7\,x\,(N-1)/4$
YValidate	$(N-1)/2+1$	$3\cdot(N-1)/4$	$7\,x\,(N-1)/4$
XTest	$3\cdot(N-1)/4+1$	$N-1$	$7\,x\,(N-1)/4$
YTest	$3\cdot(N-1)/4+1$	$N-1$	$7\,x\,(N-1)/4$

The data set having $N-1$ samples are divided into the subsets of objects conform to Table 5.

The RNN system executes a binary classification of the trajectory samples. Obviously, extreme events of the trajectory are time-dependent and can be detected based on the sequences of the sampled multidimensional time series. To keep the orbiter on the complex helicoid discussed in section III, automatic modifications were executed by the orbiter. Because of different scientific and astronomical targets of the project, there were sent modification commands of the trajectory by the human control team from the Earth, as well. For better sensing the memory behavior of the trajectory, we used LSTM layers of the neural network. Fig. 23 shows the used recurrent network.

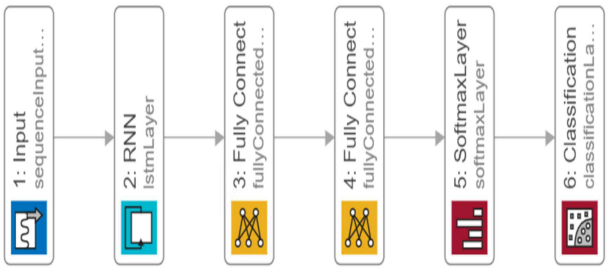

FIGURE 23. The architecture of the adopted recurrent neural network. On layer two LSTM, BiLSTM RNNs have been used with different parameters.

The output of the neural network system is a binary function indicating the appearance of the extreme modification of the Cassini orbiter trajectory. The algorithm type of neural network training is ADAM; the gradient threshold method is L2Norm. Other numerical parameters of the neural networks are given in Table 6. The number of classes is two because we use this network to detect the complex event of the trajectory. As the CED conditions (see relations 6, 7) are fulfilled for any trajectory samples, that sample is classified True, otherwise is classified False. The confusion matrix with regard to binary classification is a 2×2 table intended to depict the classification model performance. It shows precisely the number of classified samples and in which class [23].

The matrix weighs up the similarity or dissimilarity among the values of the actual target and the predicted values by the used model. The confusion matrix has four variables listed below: True positive (TP) represents the outcome at which the model accurately predicts a positive category. The

TABLE 6. Training option values of the RNN.

Option	Value
GradientDecayFactor	0.9000
SquaredGradientDecayFactor	0.9990
InitialLearnRate	0.0200
GradientThreshold	1
MaxEpochs	100
Number of Classes	2

condition is accurately identified at the time that it present. True negative (TN) gives the outcome at which the model accurately predicts the negative category. The condition is not discovered when truant. False positive (FP) represents the outcome at which the model inaccurately predicts a positive category. The condition is located without being affected by being truant. False-negative (FN) gives the outcome at which the model inaccurately predicts the negative category. The condition is not located despite having existence.

The Matthews correlation coefficient (MCC) of each RNN is calculated based on the values of the corresponding confusion matrix:

$$MCC = \frac{TP \cdot TN - FP \cdot FN}{\sqrt{(TP+FP) \cdot (TP+FN) \cdot (TN+FP) \cdot (TN+FN)}} \quad (13)$$

It can be seen that metric MCC strongly depends on the values of the confusion matrix. As the TP and TN values become larger, the numerator gives higher values. It should be mentioned that the numerator gets a high value just in case when both TP and TN have large values. Based on Lagrange multipliers can be proved that MCC gets maximum value 1 for $(TP, TN, FP, FN) = (C/2, C/2, 0, 0)$ where C is the number of elements of the data. Similarly, MCC has a minimum value -1 for $(TP, TN, FP, FN) = (0, 1, C/2, C/2)$. MCC is a metric of matching the test and predicted sets. It should be noted that metric MCC does not give high value when TN and TN are very different, and FP and FN are not close to zero.

F_1 score is calculated from the confusion matrix, but the True Negatives (TN) are neglected. The formula of the F_1 score is the following:

$$F_1 = \frac{2 \cdot TP}{2 \cdot TP + FN + FP} \quad (14)$$

F_1 score is a gauge of test precision and can be explained as both (precision and recall) weighted average [24]. It deals with both the precision and recall of the test in order to calculate the score. Precision is defined as the cardinality of the correct positive results, which are divided by the number of the whole positive results acquired by the learning model. The recall being the positive class accuracy could be defined as the proportion of pertinent samples that are accurately retrieved. In the learning framework, the precision/recall offers a beneficial intuition on the demeanor of the classifier [25].

TABLE 7. Detection accuracy of the trajectory modification of different RNNs.

RNN Type	Mini Batch Size	Hidden units# on L2	Classes# on L3	Classes# on L4	Learning time [s]	Detection accuracy [%]
$LSTM_1$	2500	10	100	2	654.2	99.86
$LSTM_2$	2500	100	100	2	749.1	99.78
$LSTM_3$	5000	10	100	2	625.9	98.39
$LSTM_4$	**5000**	**100**	**100**	**2**	**748.8**	**99.98**
$LSTM_5$	10000	10	100	2	623.2	99.92
$LSTM_6$	10000	100	100	2	748.0	99.06
$BiLSTM_7$	2500	10	100	2	1089.8	98.76
$BiLSTM_8$	**2500**	**100**	**100**	**2**	**1172.0**	**99.95**
$BiLSTM_9$	5000	10	100	2	1093.4	99.11
$BiLSTM_{10}$	5000	100	100	2	1174.7	99.19
$BiLSTM_{11}$	10000	10	100	2	1092.4	99.36
$BiLSTM_{12}$	10000	100	100	2	1175.8	98.20

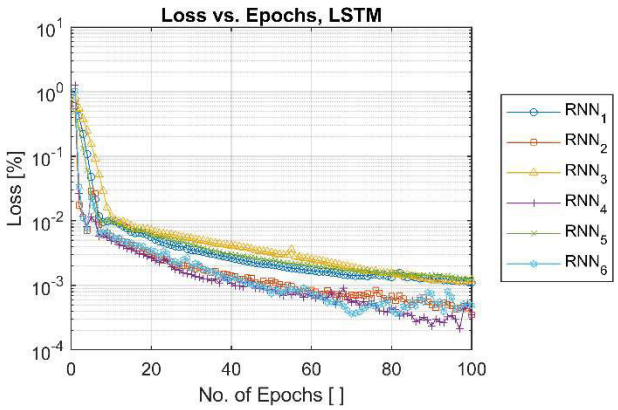

FIGURE 24. Dependence of the minibatch learning loss on the number of epochs of the RNNs-LSTM. Two decreasing phases of the loss exist.

The optimal value of the F_1 score is 1, and the lower in rank is 0. The proportional share of precision and recall are the same to F_1 score. MCC is a further trustworthy statistical evaluation, which generates a high score exclusively in the event that the acquired prediction results are good in the complete four confusion matrix classes when the positive elements size and negative elements size corresponds [26].

MCC is an exclusive rate of binary classification that achieves a high score just if we have a binary predictor that can accurately predict almost all positive data representative cases and the plurality of negative data representative cases [27], [28]. Numerous researchers have a particular opinion considering the exact meaning of F_1 score and MCC. Almost all sensible performance with standard measurements represent the ratio across the space separating the number of accurately categorized samples and the gross samples number (for instance, [29]). Two major features distinguish MCC from the F_1 score [30], [31].

Foremost, F_1 differs for category swapping. However, MCC never changes in the case that a class which is negative is renamed to be positive and vice versa. The second property, the F_1 score is detached from the number of accurately categorized samples as negative.

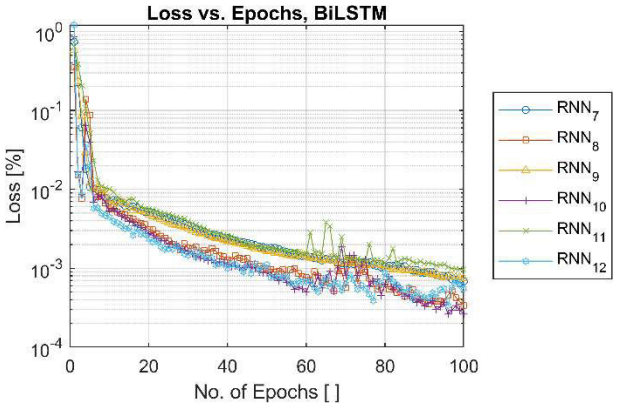

FIGURE 25. Dependence of the minibatch learning loss on the number of epochs of the RNNs-BiLSTM. Two decreasing phases of the loss exist.

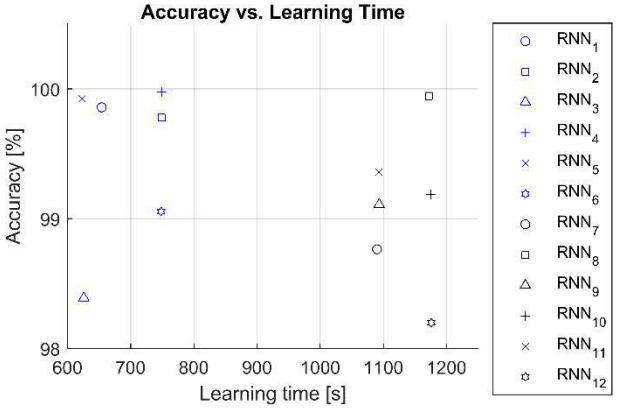

FIGURE 26. Scatter plot of the learning time and accuracy of the RNNs. RNN4 performed best at the identification of trajectory modifications.

B. EXPERIMENTAL RESULTS OF THE TRAJECTORY MANOEUVRES DETECTION

There were executed training and evaluation of the test data sets of the trajectory in the last 13.5 years of the Cassini project with twelve different recurrent neural networks. Half of them are LSTM, and the rest are BiLSTM networks. The changing input parameters (mini-batch size, number of hidden units, number of classes on layer three, and layer four). The resulting learning time and the detection accuracy of these networks are given in Table 7.

Visualization of the loss during the learning process is represented in Fig. 24. It is evident in Figure that RNN4 LSTM is providing the best loss comparing to other models. The less is the number of hidden units, the higher is the loss. For ten hidden units, we get double the learning loss. Similar behavior has both LSTM and BiLSTM networks, but the last one becomes over learned for 100 hidden units on the L2 layer.

In Fig. 25, we can notice that RNN_8 BiLSTM is providing the best loss comparing to other models. The accuracy metric is utilized in order to quantify the algorithm functioning in an explicable method. Generally, the model accuracy is specified subsequent to calculating the used model parameters with a percentage style. It is considered as the model accuracy

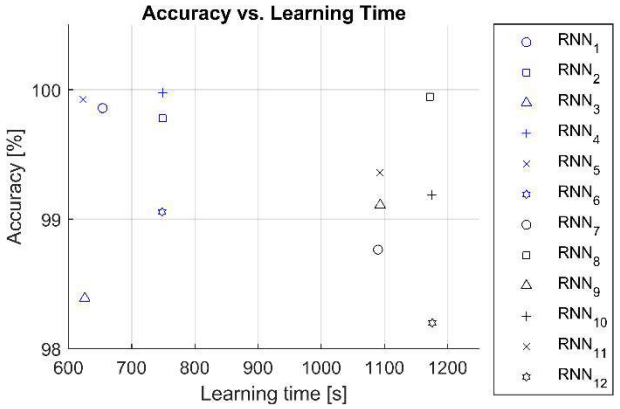

FIGURE 27. Dependency of the F_1 score on the matthew correlation coefficient *MCC*. Linear regression fits very well, showing 6% difference between the meaning of F_1 and MCC coefficient.

TABLE 8. Mathews correlation coefficient MCC and F_1 score of the analyzed RNNs.

RNN	Type	*MCC* [%]	F_1 [%]
1	LSTM	18.47	12.50
2	LSTM	13.37	7.66
3	LSTM	3.14	0.75
4	LSTM	40.04	40.00
5	LSTM	23.28	19.57
6	LSTM	4.91	1.48
7	BiLSTM	7.38	1.93
8	BiLSTM	36.91	32.50
9	BiLSTM	7.26	2.23
10	BiLSTM	9.14	2.91
11	BiLSTM	8.61	3.07
12	BiLSTM	5.03	1.11

measure that represents the model prediction contrasted to the correct data. The ideal learning rate is bound to be subjected to the loss of the leant behavior of the data, which in its role is relying on together the used dataset and the architecture of the model. The value of the loss denotes how deficiently or efficiently the model is conducting subsequent to each iteration of learning.

Fig. 26 represents the dependency of the accuracy on the learning time for each of the analyzed RNN. All LSTM networks need lower learning time than BiLSTM networks. The model accuracy is identified after calculating the used model parameters with a percentage style; this is clearly highlighted on this plot.

The dependency of the F_1 factor on the *MCC* coefficient is given in Fig. 27. It can be noted that in the case of the Cassini project, the F_1 factor is directly proportional to the *MCC* coefficient, where the slope has a value of 1.06. As an illustration, RNN4 is hitting an accuracy that exceeds the value of 99.9 % with a minimum learning time.

Mathew correlation coefficient *MCC* and F_1 score of the resulting neural networks is given in Table 8. The list of RNNs in the decreasing order of the *MCC* metric is: RNN4, RNN8,

RNN5, RNN1, RNN2, RNN10, RNN11, RNN7, RNN9, RNN12, RNN6, RNN3.

Based on this result can be assumed that the best RNN to detect trajectory modification of the Cassini orbiter is an LSTM network with MiniBatch size = 5000, 100 hidden units and is able to learn the behavior with 99.98% accuracy of the trajectory in less than 20.5 minutes on a desktop computer with 64 GB RAM and 12 CPU cores.

VI. CONCLUSION

We have provided a commencement to the expression of AI in the scope of events that are related to spacecraft trajectory modifications. Based upon this, we put forward an effective approach suitable for trajectory modifications detection via a supervised approach that utilizes the fundamental trajectory distinctive characteristics such as samples number and timing of those samples beside the spacecraft velocity. The detection method of C-H spacecraft trajectory modifications has been performed via LSTM / Bi-LSTM networks. Decisively, we show that our test analysis specifies despite the fact that the LSTM models with specific parameters establish the right choice for predicting Cassini spacecraft trajectory modifications. Their employment and extra stacked layers generate a noticeable boost in rising the detection process performance. It is worth indicating that the used models can be comfortably extended to include a considerable scientific area related to the prediction. With more specific information, the provided models present a robust processing step in employing the inner features and time-series representation via the utilization of LSTM time dependencies for precise detection. We found with our results that concerning binary classifications, MCC presents a further explanatory and veracious score than the F_1 score does. The proposed detection model is able to identify trajectory modifications of the Cassini orbiter with 99.98% accuracy.

Lastly, another main point that must be mentioned in our incoming works is the issue of outliers. The intelligent framework should consider including an anomaly detection scheme to address this issue, which we have accomplished via exploiting unsupervised algorithms to capture these extreme events or outliers. For this, a further sophisticated deep learning model should be developed. Among the collected data, images captured by the orbiter are considered as the main data origin, while the considerable defy is how to recognize and read the correct fact and information from those images.

REFERENCES

[1] M. Meltzer, "Building an international partnership and preventing mission cancellation," in *The Cassini-Huygens Visit to Saturn* (Springer Praxis Books). Cham, Switzerland: Springer, 2015, pp. 27–46.

[2] A. ALDabbas and Z. Gál, "Getting facts about interplanetary mission of Cassini-Huygens spacecraft," in *Proc. 10th Hung. GIS Conf. Exhib.*, Debrecen, Hungary, 2019, pp. 27–34.

[3] A. ALDabbas and Z. Gál, "Complex event processing based analysis of Cassini–Huygens interplanetary dataset," in *Proc. Intell. Comput. Paradigm Cutting-EDGE Technol., 1st Int. Conf. Innov. Comput. Cutting-EDGE Technol. (ICICCT)*, Istanbul, Turkey. Cham, Switzerland: Springer, 2019, pp. 51–66.

[4] G. Dematteis, T. Grafke, and E. Vanden-Eijnden, "Rogue waves and large deviations in deep sea," *Proc. Nat. Acad. Sci. USA*, vol. 115, no. 5, pp. 855–860, Jan. 2018.

[5] B. Buffington, N. Strange, and R. Ionasescu, "Addition of a low altitude Tethys flyby to the nominal Cassini tour," in *Proc. AAS/AIAA Astrodynamics Spec. Conf.*, Lake Tahoe, CA, USA. Pasadena, CA, USA: National Aeronautics and Space Administration, Jet Propulsion Laboratory, 2005, pp. 325–344.

[6] L. Spilker and S. Edgington, "Cassini-huygens: Recent science highlights and Cassini mission archive," in *Proc. EPSC-DPS Joint Meeting*, 2019, Art. no. EPSC-DPS2019.

[7] J. R. Stauch, P. Antreasian, J. Bordi, K. Criddle, R. Ionasescu, R. Jacobson, J. Jones, M. C. Meek, D. Roth, and I. Roundhill, "Preparing for the Huygens Probe Mission, Cassini orbit determination results for the first and second targeted Titan encounters," Tech. Rep. 05-2748, 2005.

[8] D. Izzo, M. Märtens, and B. Pan, "A survey on artificial intelligence trends in spacecraft guidance dynamics and control," *Astrodynamics*, vol. 3, no. 4, pp. 287–299, 2019.

[9] C. Piciarelli, C. Micheloni, and G. L. Foresti, "Trajectory-based anomalous event detection," *IEEE Trans. Circuits Syst. Video Technol.*, vol. 18, no. 11, pp. 1544–1554, Nov. 2008.

[10] L. Bontemps, V. L. Cao, J. McDermott, and N.-A. Le-Khac, "Collective anomaly detection based on long short-term memory recurrent neural networks," in *Proc. 3rd Int. Conf., Future Data Secur. Eng.*, in Lecture Notes in Computer Science, Can Tho, Vietnam, vol. 10018. Cham, Switzerland: Springer, 2016, pp. 141–152.

[11] Q. Wang, Z. Zhang, Z. Wang, Y. Wang, and W. Zhou, "The trajectory prediction of spacecraft by grey method," *Meas. Sci. Technol.*, vol. 27, no. 8, 2016, Art. no. 085011.

[12] J. Liu, H. Yu, S.-H. Cui, M. Wang, and S.-M. Li, "Spacecraft trajectory forecasting method based on induced ordered information aggregation operator," in *Proc. IEEE Chin. Guid., Navigat. Control Conf. (CGNCC)*, Nanjing, China, Aug. 2016, pp. 1618–1621, doi: 10.1109/CGNCC.2016.7829032.

[13] P. Han, W. Wang, Q. Shi, and J. Yang, "Real-time short- term trajectory prediction based on GRU neural network," in *Proc. IEEE/AIAA 38th Digit. Avionics Syst. Conf. (DASC)*, Sep. 2019, pp. 1–8.

[14] S. Silvestrini and M. R. Lavagna, "Spacecraft formation relative trajectories identification for collision-free maneuvers using neural-reconstructed dynamics," in *Proc. AIAA Scitech Forum*, 2020, p. 1918.

[15] National Aeronautics and Space Administration of the USA. *Cassini ISS Online Data Volumes, Imaging Science Subsystem (ISS), Saturn EDR Data Sets (Volume 1 - Volume 116)*. Accessed: Dec. 10, 2020. [Online]. Available: https://pds-imaging.jpl.nasa.gov/volumes/iss.html

[16] *Brent Buffington: Designing the Cassini Solstice Mission Trajectory: ASK Magazine, 15*. Accessed: Jan. 15, 2020. [Online]. Available: https://appel.nasa.gov/wpcontent/uploads/2013/04/513854main_ASK_41s_designing.pdf

[17] S. Tremaine, J. Touma, and F. Namouni, "Satellite dynamics on the Laplace surface," *Astronomical J.*, vol. 137, no. 3, pp. 3706–3717, 2009.

[18] A. LDabbas and Z. Gál, "Change detection of the Cassini orbit based on data dissimilarity," in *Proc. 11th Hung. GIS Conf. Exhib.*, Debrecen, Hungary, 2020, pp. 23–29.

[19] V. V. Yaroshenko, W. J. Miloch, S. Vladimirov, H. M. Thomas, and G. E. Morfill, "Modeling of Cassini's charging at Saturn orbit insertion flyby," *J. Geophys. Res., Space Phys.*, vol. 116, no. A12, pp. 1–13, 2011.

[20] J. Hegde and B. Rokseth, "Applications of machine learning methods for engineering risk assessment—A review," *Saf. Sci.*, vol. 122, Feb. 2020, Art. no. 104492, doi: 10.1016/j.ssci.2019.09.015.

[21] Y. Yu, X. Si, C. Hu, and J. Zhang, "A review of recurrent neural networks: LSTM cells and network architectures," *Neural Comput.*, vol. 31, no. 7, pp. 1235–1270, 2019.

[22] A. ALDabbas and Z. Gal, "On the complex event identification based on cognitive classification process," in *Proc. 10th IEEE Int. Conf. Cognit. Infocommunicat. (CogInfoCom)*, Oct. 2019, pp. 29–34.

[23] W. Taylor, S. A. Shah, K. Dashtipour, A. Zahid, Q. H. Abbasi, and M. A. Imran, "An intelligent non-invasive real-time human activity recognition system for next-generation healthcare," *Sensors*, vol. 20, no. 9, p. 2653, 2020.

[24] M. Sokolova and G. Lapalme, "A systematic analysis of performance measures for classification tasks," *Inf. Process. Manag.*, vol. 45, no. 4, pp. 427–437, 2009.

[25] M. Buckland and F. Gey, "The relationship between recall and precision," *J. Amer. Soc. Inf. Sci.*, vol. 45, no. 1, pp. 12–19, 2014.

[26] D. Chicco and G. Jurman, "The advantages of the Matthews correlation coefficient (MCC) over F1 score and accuracy in binary classification evaluation," *BMC Genomics*, vol. 21, no. 1, pp. 1–13, 2020.
[27] G. Jurman, S. Riccadonna, and C. Furlanello, "A comparison of MCC and CEN error measures in multi-class prediction," *PLoS ONE*, vol. 7, no. 8, 2012, Art. no. 41882.
[28] D. Chicco, "Ten quick tips for machine learning in computational biology," *BioData Mining*, vol. 10, no. 35, pp. 1–17, 2017.
[29] L. Wang, F. Chu, and W. Xie, "Accurate cancer classification using expressions of very few genes," *IEEE/ACM Trans. Comput. Biol. Bioinf.*, vol. 4, no. 1, pp. 40–53, Mar. 2007.
[30] Y. Sasaki, "The truth of the F-measure," *Teach Tutor Mater*, vol. 1, no. 5, pp. 1–5, 2007.
[31] D. M. W. Powers, "What the F-measure doesn't measure: Features, flaws, fallacies and fixes," 2015, *arXiv:1503.06410*. [Online]. Available: http://arxiv.org/abs/1503.06410

ASHRAF ALDABBAS received the M.Sc. degree in computer science from Al-Balqa' Applied University, As-Salt, Jordan. He is currently pursuing the Ph.D. degree with the Department of IT Systems and Networks, Doctoral School of Informatics, University of Debrecen. His research interests include sensors and sensing technology, data science, remotely sensing methods, sensor data quality assessment technique, the Internet of Things, wireless sensor networks, and deep learning. His master dissertation was entitled the award of the best dissertation for the academic year 2013/2014.

ZOLTAN GAL (Member, IEEE) graduated the engineering degree in electronics and computer science in 1990. He received the Ph.D. degree in informatics from the University of Debrecen, Hungary. He was a Chief Information Officer of the University of Debrecen for 15 year, where he is currently the Head of the Center of High-Performance Computing. He is currently an Associate Professor with the Department of IT Systems and Networks, Faculty of Informatics, University of Debrecen. He has been a Certified Professional Lecturer of the Cisco Network Academy Program since 1999. He has published over 100 scientific conference and journal articles in the field of ICT. His research interests include real-time communication, wireless broadband networks, multimedia communication, statistical analysis of high-speed packet switching, sensor networks, the Internet of Things, distributed computer systems, parallel computer architectures, and parallel computing.

KHAWAJA MOYEEZULLAH GHORI received the master's degree in computer sciences from the National University of Computer and Emerging Sciences, Pakistan, and the Ph.D. degree in computer science from the University of Debrecen, Hungary. He has been working as an Assistant Professor with the Department of Computer Science, National University of Modern Languages, Islamabad, since 2004. His research interests include machine learning, data mining, deep learning, and neutral networks.

MUHAMMAD IMRAN (Member, IEEE) received the Ph.D. degree in information technology from University Teknologi PETRONAS, Malaysia, in 2011. He is currently an Associate Professor with the College of Applied Computer Science, King Saud University, Saudi Arabia. He has completed a number of international collaborative research projects with reputable universities. He has published more than 250 research articles in peer-reviewed, well-recognized international conferences and journals. Many of his research articles are among the highly cited and most downloaded. His research interests include the Internet of Things, mobile and wireless networks, big data analytics, cloud computing, and information security. His research is financially supported by several grants. He has been involved in about more than 100 peer-reviewed international conferences and workshops in various capacities, such as the chair, the co-chair, and a technical program committee member. He has served as an Editor in Chief for European Alliance for Innovation (EAI) *Transactions on Pervasive Health and Technology*. He is also serving as an Associate Editor for top ranked international journals, such as *IEEE Network*, *Future Generation Computer Systems*, and IEEE Access. He has also served/serving as a Guest Editor for about two dozen special issues in journals, such as *IEEE Communications Magazine*, *IEEE Wireless Communications Magazine*, *Future Generation Computer Systems*, IEEE Access, and *Computer Networks*. He has been consecutively awarded with Outstanding Associate Editor of IEEE Access in 2018 and 2019 besides many others.

MUHAMMAD SHOAIB received the B.Eng. and M.Eng. degrees from the NED University of Engineering and Technology, Karachi, in 1995 and 2005, respectively, and the Ph.D. degree in communication and information system from the Beijing University of Posts and Telecommunications, China, in 2010. He worked as a Senior Manager (IP Operations, South) with Pakistan Telecommunication Company Ltd., Pakistan. He also worked as a Maintenance Engineer with R. M. International. He is currently an Associate Professor with the Information Systems Department, College of Computer and Information Sciences, King Saud University, Saudi Arabia. His research interests include video compression techniques, multilayer video coding, commercial data center facilities and IP packet-based networks, infrastructure, and security.